SSRG International Journal of Mechanical Engineering
ISSN: 2348-8360/ https://doi.org/10.14445/23488360/IJME-V12I9P112

Volume 12 Issue 9, 115-129, September 2025

Original Article

Optimizing Heat Transfer Performance of Solar Air Heaters: Influence of Hexagonal Inline and Staggered Ribs with Different Blockage Ratios in Trapezoidal Ducts

Nilesh M. Shinde[1], Himanshu Borade[2]

[1,2]*Department of Mechanical Engineering, Medi-Cap University, Indore, MP, India.*

[1]*Corresponding Author : nmshinde@outlook.com*

Received: 13 July 2025 Revised: 14 August 2025 Accepted: 15 September 2025 Published: 30 September 2025

Abstract *- Demand for energy supply is growing daily; dependency on fossil fuels is unreliable as the fossil fuels become depleted. Sustainable energy is the leading energy source for meeting global demands. Solar air heaters are one of the uses of sustainable energy. This experimental study examined the THP of a solar air heater that uses a hexagonal rib on the plate that absorbs. This study examines the effects of rib height ratio (e/Dh = 0.1109, 0.1479, and 0.1849), rib pitch (P = 60 mm, 80 mm, and 100 mm), and attack angle (α = 90° and 120°) on the transmission of heat enhancement within a trapezoidal duct for the Re of 5000-30000. To enhance the plate area and interplay of heat, trapezoidal ducts were selected. The experimental work shows that the Reynolds number leads the Nusselt number to rise for different blockage ratios. For 120° staggered ribs, with the ultimate blockage ratio, e/Dh=0.1849 performs better than all other ribs. The maximum heat transfer is higher by as much as 56% over a smooth duct, but there is more friction. The 120° rib orientation, particularly in staggered configurations, outperformed the 90° orientation. With the lowest Reynolds number, the 120° staggered rib exhibits a maximum thermal performance of 1.92, which is 29.7 percent better than the similar 90° orientation's 1.48. More thermal performance with controllable pressure losses is possible with a greater blockage ratio and a high angle of attack. In general, the absorber with hexagonal ribs improves thermal efficiency, which is a great and affordable way to make solar air heaters work better.*

Keywords *- Hexagonal ribs, Blockage ratio, Heat transfer enhancement, Convective heat transfer, Artificial Roughness.*

1. Introduction

As renewable energy sources become less available, countries need to find other ways to meet their energy needs and boost their economies. Solar energy, or isolation, is another promising option. It comes from the sun's rays. This natural, renewable resource can be used directly or changed into various forms of energy, making it a cheap, green, and flexible source of power. Solar energy is not only abundant and dependable, but it also has little influence on the environment. Throughout history, humanity has developed various innovative techniques to effectively capture and utilize solar power for everyday purposes [1-3]. An effective way to enhance heat transmission to the Air moving through the duct is to apply artificial geometry to the surface. Much research has suggested increasing the coefficient of heat transmission by introducing Roughness in the form of wires and ribs of different sizes, forms, and properties. By creating turbulence and disrupting flow, roughness geometry has been used to increase the coefficient of heat transfer. However, these adjustments will cause more frictional losses, which will make it harder to move Air through the duct. To keep frictional losses to a minimum, turbulence should only be created at the duct layer, specifically in the laminar sublayer. A lot of things affect how rough the absorber plate is and how it is organized.

The most important roughness elements are height as well as pitch. Researchers usually use dimensionless quantities, like p/e and e/D, which show the ratio of the roughness element height to the hydraulic duct diameter, to express these aspects. Among other shapes, the roughness components can be V-shaped, angled, 2D transverse, or have distinct ribs. Even though square and circular ribs are the most common, protruded, recessed, and contoured geometries are all being studied as roughness components. Nikuradse carried out the initial investigation on how Roughness affects flow and carried out several studies employing pipes roughened with sand grains to undertake

an early examination into the effect of Roughness on the transmission of velocity and the element of friction [4]. In their study of discrete double-arc ribs, Agarwal et al. [5] found that the ff and Nu were improved by about 3.07 and 3.17 times, respectively, in contrast to the smooth case, correspondingly. Chabane et al. examined the impact of locating rectangular baffles that are transverse and continuous [6]. Baffles were positioned on 30% of the absorber plate upstream, 30% downstream, and 30% in the middle. They demonstrated that adding baffles to 30% of the middle absorber plate increased thermal efficiency and decreased pressure drop. The highest THPP of 1.87 was achieved when the height-to-width ratio was 0.1 and the comparative pitch was 1.0. For uninterrupted V-shaped baffles, the optimum THPP was 2.25; for discrete V-shaped baffles, it was 2.69, according to research on the influence of pitch for both types of baffles [7]. When compared to a smooth SAH duct, the Stanton value was 1.196 times greater. The average friction factor was also found to be 1.044 times higher than that of a smooth SAH duct. The efficiency index for these integers is 1.148, which is the best [8]. Ribs of different configurations were studied for three different shapes for e/D_h=0.1, P/e= 8 to 12, and the Re is 20000. It is observed that P/e=12 has the maximum THP compared to all other P/e [9]. Ribs with decreasing height show maximum heat transfer. Numerical analysis was done on 45° V-shaped interrupted and continuous ribs, compared to 90°. V-shaped α=45° interrupted ribs show maximum thermal hydraulic performance [10].

CFD analysis of polygonal and trapezoidal ribs was studied, and the result shows that, for P/e = 10, e/D_h = 0.06, and Re=15000, a maximum THP of 1.89 was found in polygonal ribs over trapezoidal ribs [11]. When comparing the smooth absorber plate to one with different parameters, such as e/D_h = 0.043, p/e = 10, and L/w = 0.8, the Nusselt number is 6.05 times greater. Further evaluation of thermohydraulic performance yielded values between 3.24 and 3.79 [12]. CFD analysis of triangular ribs, with e/D_h=0.042, P/e=7.14, and at Re=15,000, demonstrates a maximal increase of 3.073 in the Nusselt number. Furthermore, it was noted that the greatest friction factor was 3.356. Thermal hydraulic performance was observed between the range of 1.36 and 2.11 [13]. Over a smooth duct, the maximum Nusselt number is 2.747 and the friction factor is 3.404 for a T-inverted form rib with P/e=7.14 and Re=15000. Thermal performance was found to be 1.87 [14]. NACA profile ribs at 30° α, 0.167 g/l, and 1.333 w/e, the highest thermal performance was 2.65 and 2.578 [15]. A pentagonal rib's numerical simulation with heat transport reveals 101% far more than the smoother one at Re = 15000, e/Dh = 0.05, and P/e = 10, with a frictional penalty of 2.97 at e/D_h = 0.05, P/e = 10, and Re = 4000. The highest THP found was 1.46, with P/e, e/D_h are 10, 0.05 [16]. D-shaped ribs were numerically studied for r/P_t=0.1 to 0.35, P_l/r=4-10, and Re=10200-20200. D-shaped maximum thermal performance was found at 1.12 at r/P_t = 0.25 and P_l/r = 4. [17]. A triangular duct with V-rib with R_p = 10, R_h = 0.05, Re = 7000, and α = 45° found a maximum effectiveness of 2.01 [18]. Multi V-type ribs with α=30-75°, e/D=0.019-0.043, P/e=6-12, and Re=2000-20000; W/w=6 were shown to have the best thermal performance. It emerged that the Nu and ff were six to five times over an even plate [19]. The maximum value of thermal performance for a V-shaped rib is found at 60°. Evaluated the impact of the attack angle, the quantity of transverse V-ribs, and various geometric attributes of V-shaped ribs. [20]. Delta-shaped ribs with P_l/e=3/2 show maximum heat transfer. An angle of occurrence of 30-60° shows maximum THP compared to previous research [21]. Roughness in cubicles on the absorber plate with P/e=20 and w/e=8 shows optimum thermal performance. The Nusselt number achieves its maximum improvement, 72.7%, with the friction factor found to be 138.7% [22].

Numerical analysis of stepped cylindrical turbulators with Re=18000 gives maximum thermal performance of 1.49 [23]. Conical generators with staggered fashion attached to the absorber plate, numerical simulation with Re=3000-16000, e/D_h=0.17-0.34, P/e=2.67-15, and THP found at 2.04 [25]. The impact of geometrical features on the efficacy of solar air heaters was examined with Re=3000-27000. P/g = 3.4 to 3.8, and e/D_h = 0.3 to 0.7. It was found that maximum thermal performance was found at p/g=3.8 and e/D_h=0.6, which is 2.67 times that of a smooth surface [26]. Numerical investigation of C-shape, reverse C-shape, and reverse R-shape, with P/e=14.285, e/D=0.021, and Re=4000-18000, reveals that the Nusselt number (Nu) and friction factor (f) increase by factors of 2.5 to 3.3 and 2.8 to 5.05, respectively, compared to a smooth duct. Maximum thermal performance was found at the C-shaped rib, which is 2.00 times better than all other ribs [27]. A cylindrical-shaped rib with d/H = 0.055, e/H = 0.053, L/H = 0.192, and S/H = 0.158 was found to have maximum thermal performance at 1.20 [28]. Improving the efficacy of the solar air heater with a 3D cylindrical-shaped rib with W/B=5, h/D=0.06, and Re=3000-8000 shows a maximum Nu of 69.7% with a ff of 171.3% over a smooth plate [29]. A 64.5% gain in the Nu and a 153.3% rise in the ff were noted at Re = 8000, p/e = 10, and w/e = 4. The conical Roughness demonstrates a thermo-hydraulic efficiency index of 0.8233, observed at p/e = 20 and w/e = 8 with a Reynolds number of 3000. [30]. Inclined spherical ball roughness was tested for different $\dot{m}$ of 0.0372, 0.0391, 0.04, and 0.0418 kg/s. Maximum thermal efficiency was found to be 81% over the smooth surface [31].

Many researchers have worked on different geometries with varying pitch to height, relative height to diameter, pitch to gap, and different angles of attack. Table 1 shows a relative evaluation of multiple rib types. Many ribs exhibit maximum THP, albeit at the expense of a pressure decrease.

To overcome these losses and maximize the heat transfer rate, current research work is on hexagonal-shaped ribs with different blockage ratios in trapezoidal ducts. Three different blockage ratios of hexagonal ribs arranged in inline and staggered configurations, with angles of attack α=90-120°. Evaluate the performance of these ribs by comparing them to a smooth plate. Investigating and modifying these geometries can considerably improve SAH's effectiveness and efficiency, which will help create sustainable energy solutions.

Table 1. This study's results are compared to those of others, emphasizing variations and performance advancements.

Ref.	Geometry of rib	Parameters	Result
[8]	Wire-shape	W/H = 5, h/D = 0.01, p/h = 40, α = 50° Re 3000-8000	The St is 80.6%. The highest efficiency index is 1.14.
[9]	Square, Triangular, Trapezoidal	e/D_h=0.1, P/e= 8 to 12. Re=20000	P/e=12 has maximum THP. Trapezoidal ribs that descend transfer the most heat.
[10]	V-shape interrupted & continuous	Re=10000-40000 α = 45◦-90◦	The 45◦ V-shaped continuous showed maximum THP.
[11]	Polygonal and Trapezoidal	P/e=3.33-20, e/D_h=0.03-0.09 Re=3800-18000	The maximum THP found was 1.89 in the polygonal rib.
[12]	Trapezoidal	L/w=0.2–1.0, e/D_h=0.023-0.054, P/e=6–12, α=60° Re=2000–16000	Maximum THP found in the range of 3.24–3.79.
[13]	Triangular	Re=3800-18000, P/e=7.14-35.71, e/d=0.021-0.042	Maximum THP found in the range of 1.36 and 2.11.
[14]	Transverse inverted-T	P/e=7.14-17.86, Re=3800-18000	Maximum THP found 1.87.
[15]	NACA Profile	α=15°–90°, g/l=0.143-0.333, w/e=0.667-1.667, Re=6000-18000.	Maximum THP found in the range of 2.65 and 2.578.
[16]	Pentagonal shape	P/e=6-12, e/D_h=0.03-0.05, Re=4000-18000	Ideal THP found 1.46.
[17]	D-shape	r/P_t=0.1 to 0.35, P_l /r=4 to 10, Re=10200-20200.	Maximum THP found 1.12.
[18]	V-shape	R_p = 10, R_h = 0.05, Re=5000-20000 α = 45°	Maximum effectiveness found 2.01.
[19]	V-shape	Re=2000- 20000 e/D=0.019-0.043, P/e=6-12, α=30–75° W/w= 1–10.	Maximum THP found at W/w = 6.
[21]	Delta-shape	Re=2100-30000 e/H=0.25-0.75, Pl/e= 3/2-11/2, Pt/b= 1-7/3, α=30° to 90°.	Maximum THP found at Pl/e=3/2.
[22]	Cubical	Re=3000-8000, P/*e*= 10-20, *w*/*e*=4-8, e/D_h=0.06, *W*/*H*=5	The ideal efficiency is 0.811.
[23]	Stepped cylindrical	Re=3000-24000, P/e= 11.11, 16.67, 22.22, and 27.78,	Maximum THP found 1.49.
[25]	Conical vortex	P/e=2.67-15,	Maximum THP found 2.04.

		e/D_h=0.17-0.34, Re=3500-16000	
[26]	Staggered C-shape	Re=3000-27000 P/g= 3.4 to 3.8, e/D_h= 0.3 to 0.7	The THP was achieved p/g=3.8, e/D_h=0.6.
[27]	C and R Shape	P/e=14.285, e/D=0.021. Re=4000-18000	C-shaped ribs found a maximum THP of 2.00, more than the other ribs.
[28]	Cylindrical shape	d/H = 0.055, e/H = 0.053, L/H = 0.192, and S/H =0.158	Maximum THP found 1.20
[29]	3D cylinder shape	W/B=5, h/D=0.06, Re=3000-8000.	Average ff increases by 171.3 %, and Average Nu increases by 69.7 %.
[30]	Conical Shape	Re=3000-8000, P/e=10-20, w/e=4-8, e/D_h=0.08, α=90°,	Thermo-hydraulic efficiency index found 0.8233
[31]	Inclined Spherical ball	m= 0.0372, 0.0391, 0.04 and 0.0418 kg/s	Maximum thermal efficiency found 81 %

2. An Experimental Evaluation of a SAH

To conduct an investigation into the effects of hexagonal ribs on fluid flow and heat transfer in a trapezoidal duct, considering operational conditions, an experimental setup has been planned and erected (Figures 1, 2, and 3) in accordance with ASHRAE standards (1977), which took into account practical system parameters.

A wooden duct with three segments— A starting segment, a testing segment, and a departure segment- makes up the experimental setup. The absorber plate is made of aluminum grade 6063, which has k=201-218 W/m. K is 1.0 meters long, 0.3 meters wide, and 0.03 meters high. On the lower plate of the sheet are artificially roughened hexagonal ribs with inline and staggered orientations, with different blockage ratios.

Two halogen bulbs that are 500 watts each are utilized to provide a steady heat flux of 1000 W/m². (Figures 1 and 3) display the block diagram of the experimental setups and the hexagonal rib configuration, respectively. Fast-drying epoxy is used to attach the roughness ribs securely to the bottom of the absorber sheet. Table 2 shows a list of the equipment and operational variables for the experiment. In accordance with the literature survey, the pitch-to-height ratio between 8 and 10 was observed to be best for attachment and reattachment of the boundary layer. Based on this, P/e=10 taken for this experiment.

A power blower, a halogen bulb, a digital anemometer (Model: GM816), a digital pressure gauge, a metal galvanized pipe, valves for control, a data logger, and calibrated thermocouples are among the layout's main components. To measure temperatures at different places using RTD (PT-100) thermocouples connected to a data logger. Using different blockage ratios and angles of attack, the experiment aimed to collect information about the friction factor and the heat flow. To confirm that all of the major components, including the digital data logger, digital manometer, and digital anemometer, performed as intended, we looked at a range of roughness parameters. For every roughened sheet, we obtained five flow rate readings and adjusted them using control valves.

All the results have been recorded after adjusting the flow rate and allowing the system to stabilize. Throughout the entire experiment, we recorded the air and plate temperatures, the pressure drops in the duct, and the digital manometer. “Quasi-steady state” refers to the temperature at the absorber surface and outlet air remaining the same for twenty minutes. In the initial stages, each test run took about two to three hours to reach a steady state.

Table 2. Operating parameters for the experiment

Parameters	Values
Reynolds No. (Re)	5000-30000
Pitch to Depth ratio (P/e)	10
Blockage Ratio e/D_h	0.1109, 0.1479 and 0.1849
Angle of attack (α)	90°, 120°
Aspect ratio (W/H)	10.57
Hydraulic diameter (D_h)	0.05408
Rib distance (P)	60 mm, 80 mm, and 100 mm
Height of rib (e)	6 mm, 8 mm, and 10 mm
Heat flux, I	1000 W/m^2
Absorber Plate Material	Aluminium
Length of test section	1 m

Table 3. Uncertainty of devices used in the experimental setup

Device	Typical Uncertainty
Digital Anemometer	±2 % – ±5 % of reading
Digital Manometer	±1 % – ±2 % of reading
Data Logger	±0.5 ◦C – ±0.1 ◦C
AC Motor + Blower	Minor speed fluctuation
Toggle switch, regulating valve, GI pipe, duct sections.	Negligible direct uncertainty

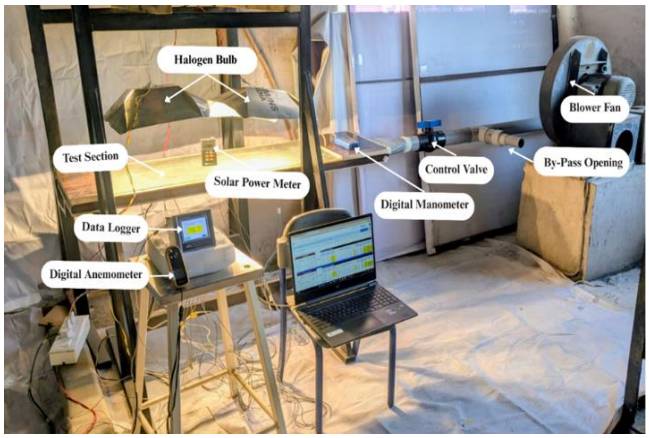

Fig. 1 Experimental Setup

Fig. 2 Roughness rib geometrical view displaying different heights

Depending on the observed parameter and the specific operating conditions, the total experimental error is projected to be between ±2% and ±5% when taking into account the unique uncertainties of the instruments used.

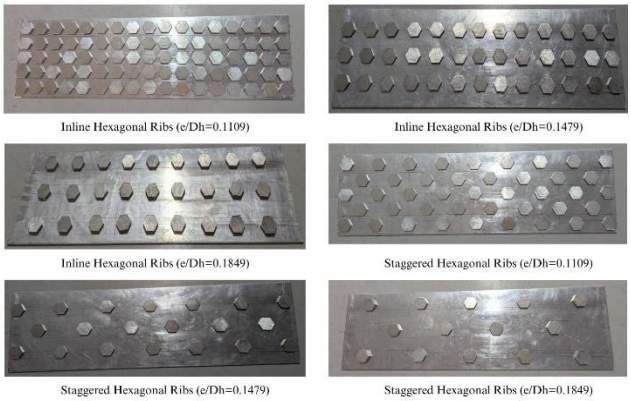

Fig. 3 Inline and staggered arrangement for 120° with e/Dh= 0.1849, 0.1479, 0.1109.

3. Measurement Techniques and Performance Evaluation

Several tools were used to record the experimental readings for varying roughness components with different blockage ratios on the absorber plate. The data acquired from the rough and smooth sheets were compared after A control valve was employed to adjust the air flow rate. Nusselt number, friction factor, heat transfer coefficient, and THP were computed using this experimental data.

3.1. Data Reduction

3.1.1. The Average Temperature of the Plate (T_{pm})

$$Absorber\ plate\ mean\ temperature, Tpm = \frac{T_1 + T_2 + T_3 + T_4 + T_5 + T_6 + T_7 + T_8 + T_9 + T_{10} + T_{11}}{11} \quad (1)$$

3.1.2. Mean Temperature of Plate (T_{pm})

$$Air\ mean\ Temperature\ T_{fm} = \frac{T_i + T_o}{2} \quad (2)$$

3.1.3. Hydraulic Diameter

$$D_h = \frac{4 \times W \times H}{2(W + H)} \quad (3)$$

3.1.3. Heat gained by Air

$$Q = \dot{m} C_p (T_0 - T_i) \quad (4)$$

3.1.4. Convective Heat Transfer Coefficient from Newton's Law of Cooling

$$h = \frac{Q}{A_P (T_{Pm} - T_{fm})} \quad (5)$$

3.1.5. Nusselt Number

$$Nu = \frac{hD_h}{K} \quad (6)$$

3.1.6. Friction Factor

$$f = \frac{\Delta P \times D_h}{2 \times \rho \times L \times V^2} \quad (7)$$

3.1.7. Friction Factor

$$THP = \frac{Nu/Nu_s}{(f/f_s)^{1/3}} \quad (8)$$

4. Experimental Validations

Trials on a straight conduit verified the test configuration before collecting data. After comparing the predicted outcomes from Equations (9) and (10), the trials gave f and Nu values. A smooth trapezoidal duct's f value is obtained by the modified Blasius equation:

$$f_{th} = 0.085\ (Re)^{-\frac{1}{4}} \quad (9)$$

The Dittus-Boelter equation calculates Nu for smooth trapezoidal ducts.

$$Nu_{th} = 0.023Re^{0.8}Pr^{0.4} \quad (10)$$

The impact of different flow configurations and surface roughness characteristics on airflow heat transfer in a trapezoidal duct is examined experimentally in this work. To evaluate enhancements in the h, Nu, and f, the performance of various roughness parameters is contrasted in conjunction with that of a smooth duct under analogous flow circumstances. While Figure 4 shows the experimental trend of an increase in Nusselt Number with a higher Reynolds number (Re), Table 4 summarizes the reported improvements in the heat transfer coefficient. Also, Figure. 5**)** shows the experimental trend of a decrease in friction factor with a higher Reynolds number (Re), and Table 5 summarizes the reported friction factor values.

Table 4. Comparison of experimental and theoretical Nusselt numbers across Reynolds numbers for a smooth plate

Sr. No	Reynolds Number	Nu_{exp}	Nu_{th}
1	10081.75	34.58	31.886
2	15122.62	48.35	44.105
3	20163.5	60.66	55.521
4	25204.37	72.87	66.374
5	29300.09	81.31	74.872

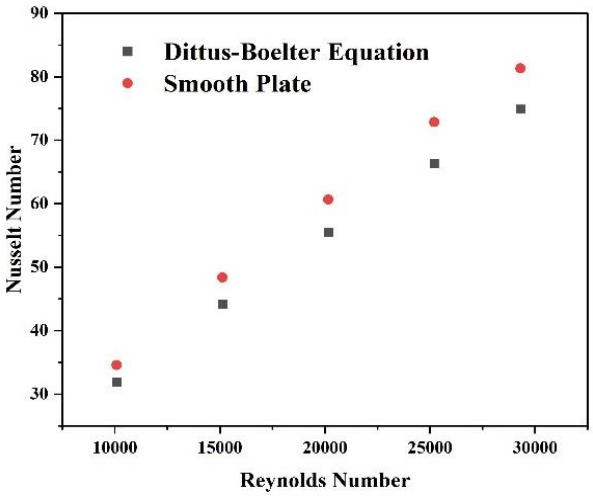

Fig. 4 Nusselt number vs. Reynolds number for smooth plate

Table 5. Comparison of experimental and predicted friction factors over Reynolds numbers for a smooth plate.

Sr. No	Reynolds Number	f_{exp}	f_{th}
1	10081.75	0.0349	0.0316
2	15122.62	0.0316	0.0285
3	20163.5	0.0293	0.0266
4	25204.37	0.0277	0.0251
5	29300.09	0.0268	0.0242

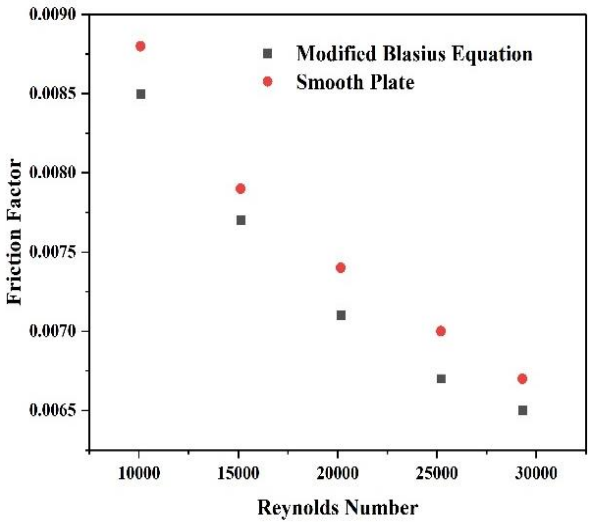

Fig. 5 Friction factor vs Reynolds number for smooth plate

5. Results and Discussion

5.1. Influence of Reynolds Number on Nusselt Number

In this experimental setup, the Reynolds number varies between 5000 and 30000. The absorber plate is equipped with hexagonal inline and staggered ribs with an angle of attack α=90-120°.

They were studied to examine the effects of the Re on different blockage ratios of hexagonal ribs. Experimental findings show that the Nusselt number is augmented with an elevation in the Reynolds number.

Convective transfer of heat is augmented due to attachment and reattachment of Air for P/e=10, which causes the disruption of boundary layers. This process results in adequate aeration. In this context, a staggered rib arrangement performs better than an inline rib arrangement.

At Reynolds numbers above 20,000, the overall THP was still advantageous, particularly in staggered arrangements. These results show improved heat transfer results from higher Reynolds numbers, but the penalty of pressure drop calls for careful design consideration.

For the 90° rib arrangement, Nu increases with the Re and blockage ratio. At Re = 10081.75, the Nusselt number rises from 34.58 (smooth) to 49.83 (BR=0.1849, inline) and 70.18 (BR=0.1849, staggered), indicating 44.1% and 102.9% enhancement, respectively.

At Re = 20163.5, the inline Nusselt numbers are 69.56 (BR=0.1109), 73.76 (BR=0.1479), and 76.86 (BR=0.1849), while the staggered arrangement shows 84.84, 92.41, and 97.21, up to 60.3% higher than the smooth value. At the maximum Re = 29300.09, the staggered (BR=0.1849) achieves 118.46, which is 45.7% higher than smooth, while the inline (BR=0.1849) reaches 98.11 (20.7% higher).

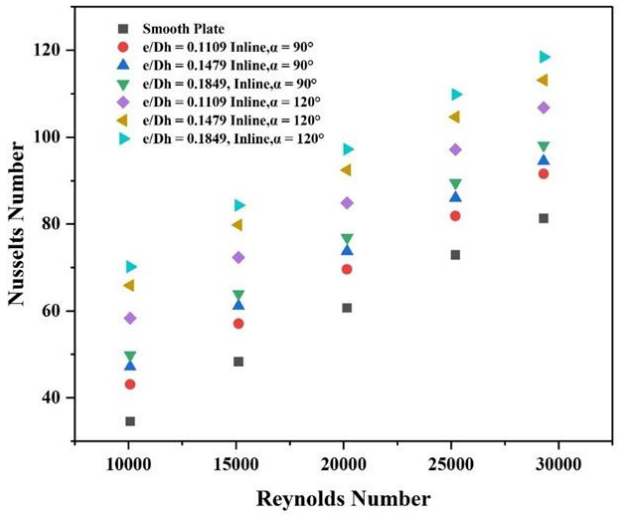

Fig. 6 Nusselt number vs. Reynolds number for 90°-120° inline configuration

For the 120° ribs, a similar increasing trend is observed, but with greater Nusselt numbers across all conditions. At Re = 10081.75, the inline (BR=0.1849) results in 60.01, and the staggered (BR=0.1849) results in 91.46—73.6% and 164.5% higher than smooth (34.58). At Re = 20163.5, staggered ribs show 97.55 (BR 0.1107), 108.76 (BR=0.1479), and 118.49 (BR=0.1849), which is up to 95.4% higher than the smooth case. At Re = 29300.09, the highest Nusselt number reaches 139.74 (BR=0.1849, staggered), which is 72% more than smooth, while inline (BR=0.1849) reaches 108.29 (33.2% higher).

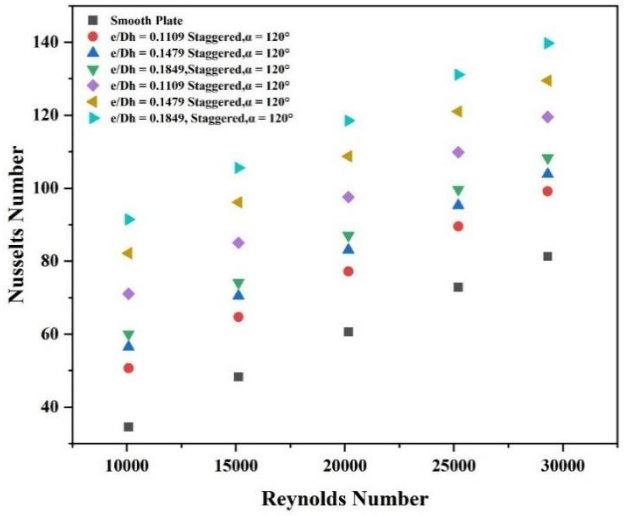

Fig. 7 Nusselt number vs. Reynolds number for 90°-120° staggered configuration

The 120° staggered ribs consistently outperform the 90° ones. For instance, at Re = 29300.09 and (BR=0.1849), the Nusselt number for 120° staggered is 139.74, compared to 118.46 for 90°, showing an 18% improvement. Inline 120° also performs better than 90°, at Re = 20163.5, it provides 87.04 vs. 76.86. Overall, the 120° orientation—especially with staggered ribs and higher blockage ratios—demonstrates greater efficacy in augmenting convective heat transfer owing to heightened turbulence and improved disruption of the thermal boundary layer.

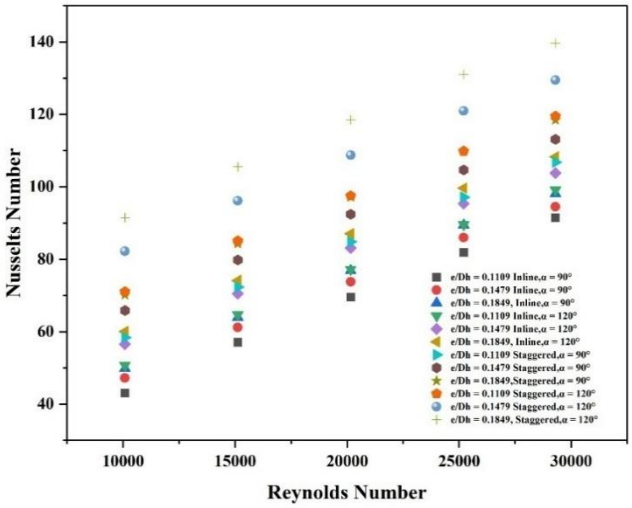

Fig. 8. Nusselt number vs. Reynolds number for 90°-120° inline and staggered configuration

5.2. Effect of Reynolds Number on Friction Factor

The friction factor diminishes as the Reynolds number increases for all blockage ratios in the 90° rib configuration. At Re = 10081.75, the friction factor increases from 0.0088 (smooth) to 0.020 (BR=0.1849, inline) and 0.023 (BR=0.1849, staggered), showing a 127% and 161% rise, respectively. As Re increases to 20163.5, the inline values drop to 0.0105 (BR=0.1107), 0.012 (BR=0.1479), and 0.014 (BR=0.1849), while staggered ribs show 0.0145, 0.015, and 0.016 - still significantly higher than the smooth case (0.0074). At Re = 29300.09, the maximum ff observed is 0.015 (BR=0.1849, staggered), compared to 0.0067 for the smooth duct.

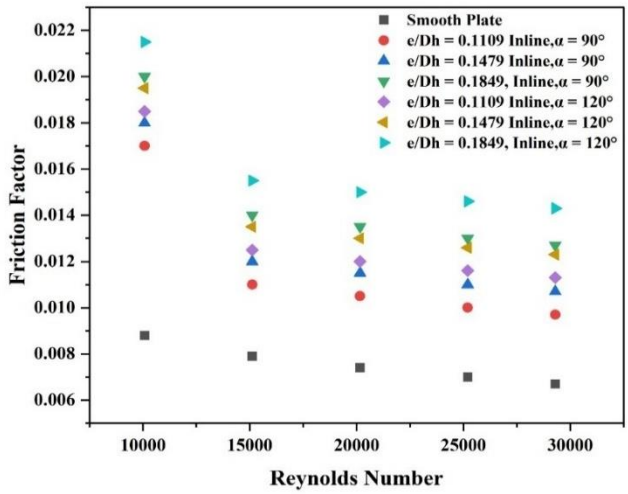

Fig. 9 Friction factor vs. Reynolds number for 90°-120° inline configuration

The 120° rib setup exhibits similar decreasing trends, albeit with comparatively lower friction factors. At Re = 10081.75, the inline (BR=0.1849) result in a friction factor of 0.0215 (vs. 0.023 for 90°), and the staggered (BR=0.1849) yields the same 0.023. However, at higher Reynolds numbers, the 120° setup shows lower resistance. For instance, at Re = 20163.5 and (BR=0.1479), the staggered 120° rib shows 0.0155 compared to 0.016 for 90°. At Re = 29300.09 and (BR=0.1849), the staggered value is 0.0157- slightly higher than inline (0.0143), yet still comparable to 90°.

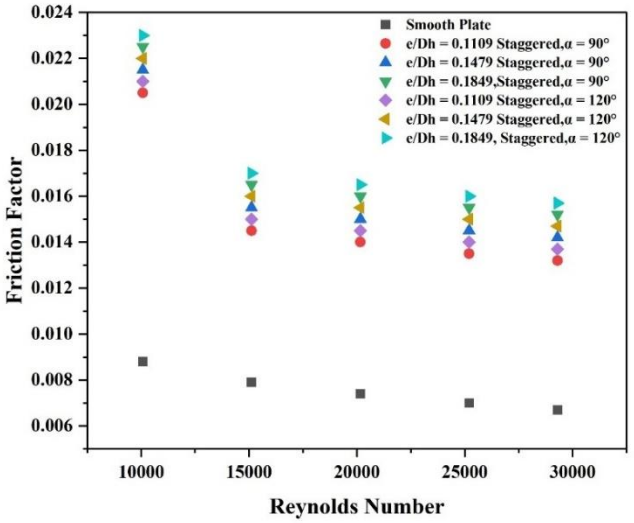

Fig. 10 Friction factor vs. Reynolds number for 90°-120° staggered configuration

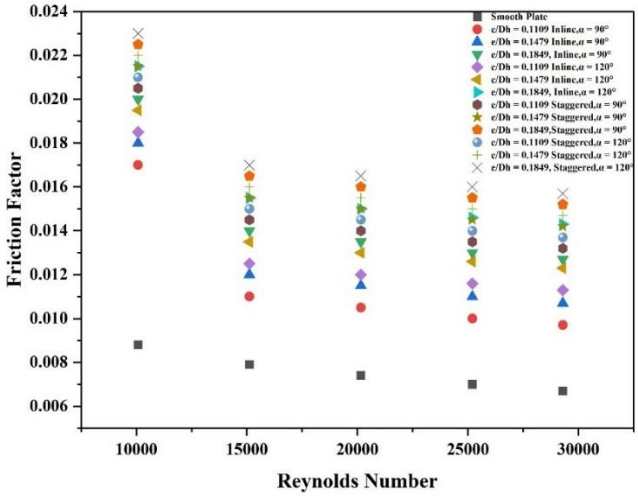

Fig. 11 Friction factor vs. Reynolds number for 90°-120°iInline and staggered configuration

While both rib orientations increase friction compared to a smooth duct, the 120° configuration generally shows marginally lower friction factors than the 90° setup, especially at higher Reynolds numbers. This suggests that the 120° ribs provide an optimal equilibrium between the augmentation of heat transmission and the resistance to flow. For Re = 25204.37 and (BR=0.1849), the 90° staggered configuration yields 0.016, while the 120° configuration gives 0.016 as well, but with a better Nusselt number. Therefore, 120° ribs are more efficient for applications seeking improved heat transfer with relatively moderate pressure drops.

5.3. Effects of Blockage Ratio

The Blockage Ratio (BR) considerably affects both thermal conduction and flow resistance. As BR increases from 0.1107 to 0.1849, the Nusselt number shows a consistent rise, indicating enhanced turbulent transfer of heat due to increased turbulence and interruption of flow. For instance, in the 120° staggered arrangement at Re = 20163.5, the Nusselt number increases from 97.55 (BR 0.1107) to 108.76 (BR=0.1479) and 118.49 (BR=0.1849), demonstrating a 21.5% enhancement between BR 0.1107 and 0.1849. Similarly, for the 90° inline case at Re = 25204.37, the Nusselt number increases from 81.87 (BR 0.1107) to 89.47 (BR=0.1849), a gain of 9.3%.

However, this thermal improvement is accompanied by an increase in the friction factor. At Re = 10081.75 in the 90° staggered configuration, the friction factor rises from 0.021 (BR 0.1107) to 0.023 (BR=0.1849), a 9.5% increase. In the 120° inline case at Re = 20163.5, the friction factor increases from 0.012 (BR 0.1107) to 0.015 (BR=0.1849), or about 25%. This trend confirms that higher blockage ratios enhance heat transfer and impose greater pressure penalties. Therefore, selecting an optimal BR involves balancing thermal performance with acceptable flow resistance based on system requirements.

5.4. Effects of Blockage Ratio

The angle of attack significantly affects heat transfer enhancement and flow resistance in ribbed ducts. Comparing 90° and 120° rib orientations reveals that increasing the angle to 120° consistently improves the Nusselt number across all Reynolds numbers and blockage ratios. For instance, at Re = 20163.5 and (BR=0.1849) in the staggered configuration, the Nusselt number rises from 97.21 (α=90°) to 118.49 (α=120°), an increase of 21.9%. Similarly, at Re=29300.09 and (BR=0.1849), the staggered α=120° arrangement achieves a Nusselt number of 139.74, compared to 118.46 for α=90°, marking an improvement of 17.9%. This enhancement is attributed to stronger secondary flow and better boundary layer disruption at higher attack angles.

In terms of friction factor, the α=120° orientation generally exhibits slightly lower or comparable values to the α=90° configuration, especially at higher Reynolds numbers. At Re = 25204.37 and (BR=0.1849), the friction factor for staggered ribs is 0.016 in both α= 90° and 120° configurations. However, at Re = 20163.5 and

(BR=0.1479), the friction factor reduces from 0.016 (α=90°) to 0.0155 (α=120°) in staggered ribs. This indicates that increasing the angle of attack enhances thermal performance without significantly increasing pressure losses. Overall, the α=120° rib orientation offers a better compromise between thermal conduction and fluid resistance, making it a more efficient choice for thermal system design.

5.5. Thermal Performance

Rib orientation, blockage ratio, and Reynolds number significantly influence thermal performance, which balances heat transfer enhancement against pressure drop. Staggered ribs consistently exhibit higher thermal performance than inline ribs across all configurations. For Re = 10081.75 and (BR=0.1849), the thermal performance for α=90° staggered reaches 1.48, while α=120° staggered achieves 1.92, indicating a 29.7% improvement due to the change in angle. Likewise, at Re = 15122.62 and (BR=0.1479), the performance increases from 1.32 (α=90° staggered) to 1.57 (α=120° staggered), a gain of 18.9%.

Thermal performance remains close to 1.0 for inline arrangements, with slight variations. In the α=90° inline setup at Re = 29300.09, the values drop below unity (0.99 to 0.97), indicating diminished benefit at higher Reynolds numbers. Conversely, α=120° inline retains better performance, staying above 1.0 up to the highest Re. The α=120° staggered configuration with (BR=0.1849) consistently shows the highest thermal performance, reaching 1.69 to 1.92 across the Reynolds range. This data demonstrates that the combination of a higher angle of attack and staggered rib arrangement enhances heat transfer more effectively without proportionally increasing friction losses. Thus, α=120° staggered ribs with larger blockage ratios offer optimal thermal performance for turbulent duct flows.

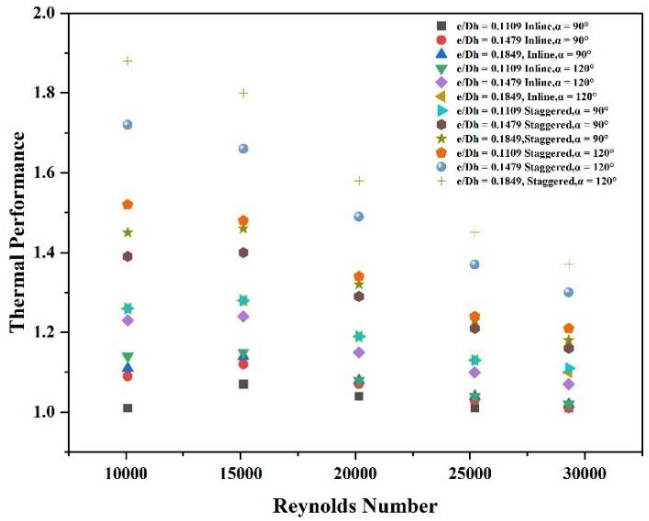

Fig. 12 illustrates the thermal performance compared to the Reynolds number for both (α=90°-120°) inline and staggered configurations

6. Conclusion

The experimental result shows that both rib orientation and blockage ratio have an immense effect on thermal conduction and direction of flow. The angle of attack α=90° to 120° results in improved Nusselt number with increased convective heat transfer. The staggered configuration showed pronounced enhancement over the inline configuration.

- For the highest Reynolds number (Re = 29300.09) and blockage ratio (BR=0.1849), the Nusselt number improves from 118.46 in 90° staggered to 139.74 in 120° staggered, a gain of approximately 17.9%.
- As the blockage ratio rises, the friction factor falls, and vice versa as the Reynolds number rises. The maximum friction factor observed at the highest Reynolds number (Re = 29300.09) is 0.015 with (BR=0.1849, α=120°staggered), compared to 0.0067 for the smooth duct.
- Thermal performance, the equilibrium between heat transfer and pressure loss, is highest for the 120° staggered ribs, especially at lower Reynolds numbers and higher blockage ratios. At the lowest Reynolds number (Re = 10081.75) and (BR=0.1849), the thermal performance reaches 1.92, compared to 1.48 in the 90° staggered configuration.
- Inline configurations show modest gains, but staggered ribs consistently outperform due to more effective boundary layer disruption.

Overall, the 120° staggered configuration with higher blockage ratios (BR=0.1849) delivers the best thermal performance. This rib configuration is the best for increasing heat transmission, with manageable pressure losses in turbulent duct flows.

6.1. The Future Scope and Applications of this Study

Thermal management of various instruments required minimized power loss while achieving the highest convective heat transfer coefficient. The current idea regarding using hexagonal ribs with different blockage ratios and attack angles is efficient for handling the heat conduction and minimizes the pressure drop. The augmented surface on the absorber plate creates secondary flow, which causes proper flow mixing and thermal distribution. This approach will help in various fields. This design can be used in a number of places, such as:

- Electronic devices get heated by continuous operating, for which proper ventilation of heat is required. Proper heat removal will increase the performance and life of equipment.
- Industrial heat exchangers: Efficiency and performance will depend on less energy consumption and maximum output. This design will help improve proper heat transfer and efficiency.
- In the automotive and aerospace industries, the cooling

of the engine is an important factor for its efficiency. This will make parts get heated. Performance can be increased by using this design.

- Heating, ventilation, and air-conditioning systems help make places cool, and their efficiency depends on how efficiently they remove heat from the building design. This study will help achieve the proper building design to achieve maximum cooling effects.

Future research may concentrate on modifying this geometry for other scales, materials, and climatic circumstances, facilitating further progress in the domain of thermal engineering.

Despite the examination of numerous roughness characteristics, our understanding of the precise impacts of supplementary geometric configurations on heat transmission and overall system efficacy remains inadequate. Filling this gap could help us learn how to improve roughness design, which would lead to better thermal performance and cheaper solar energy systems. More research, such as CFD analysis and sophisticated rib geometry, is needed to determine how and why different roughness geometries work and their benefits. These discoveries will help the field move forward and lead to real-world uses.

Acknowledgment

The authors would like to thank Medi-caps University, Indore, and R. C. Patel Institute of Technology, Shirpur, for the support.

Author Contributions

Ideas, procedures, first drafts, preparation, data curation, investigations, reviews, edits, formal analysis, and visualization are all handled by Nilesh M. Shinde. The project administration is overseen by Dr Himanshu Borade.

References

[1] Abdulmohsen O. Alsaiari et al., "Heat Transmission and Air Flow Friction in a Solar Air Heater with a Ribbed Absorber Plate: A Computational Study," *Case Studies in Thermal Engineering*, vol. 40, pp. 1-9, 2022. [CrossRef] [Google Scholar] [Publisher Link]

[2] Harish K. Ghritlahre, and Radha K. Prasad, "Prediction of Exergetic Efficiency of Arc Shaped Wire Roughened Solar Air Heater Using ANN Model," *International Journal of Heat and Technology*, vol. 36, no. 3, pp. 1107-1115, 2018. [CrossRef] [Google Scholar] [Publisher Link]

[3] Rahul Kumar et al., "Experimental Assessment and Modeling of Solar Air Heater with V Shape Roughness on Absorber Plate," *Case Studies in Thermal Engineering*, vol. 43, pp. 1-9, 2023. [CrossRef] [Google Scholar] [Publisher Link]

[4] J. Nikuradse, "*Laws of Flow in Rough Pipes*," National Advisory Committee for Aeronautics, Report, pp. 1-63, 1950. [Google Scholar] [Publisher Link]

[5] Yogesh Agrawal et al., "Investigation of Thermal Performance of a Ribbed Solar Air Heater for Sustainable Built Environment," *Sustainable Energy Technologies and Assessments*, vol. 57, 2023. [CrossRef] [Google Scholar] [Publisher Link]

[6] Foued Chabane et al., "Experimental Study of a Solar Air Heater by Adding an Arrangement of Transverse Rectangular Baffles Perpendicular to the Air Stream," *International Journal of Green Energy*, vol. 16, no. 14, pp. 1264-1277, 2019. [CrossRef] [Google Scholar] [Publisher Link]

[7] Kottayat Nidhul et al., "Thermo-Hydraulic and Exergetic Performance of a Cost-Effective Solar Air Heater: CFD and Experimental Study," *Renewable Energy*, vol. 184, pp. 627-641, 2022. [CrossRef] [Google Scholar] [Publisher Link]

[8] Hani Abulkhair et al., "Heat Transfer and Air Flow Friction in Solar Air Heaters: A Comprehensive Computational and Experimental Investigation with Wire-Roughened Absorber Plate," *Case Studies in Thermal Engineering*, vol. 48, pp. 1-18, 2023. [CrossRef] [Google Scholar] [Publisher Link]

[9] R. Kamali, and A.R. Binesh, "The Importance of Rib Shape Effects on the Local Heat Transfer and Flow Friction Characteristics of Square Ducts with Ribbed Internal Surfaces," *International Communications in Heat and Mass Transfer*, vol. 35, no. 8, pp. 1032-1040, 2008. [CrossRef] [Google Scholar] [Publisher Link]

[10] Wei Peng et al., "Experimental and Numerical Investigation of Convection Heat Transfer in Channels with Different Types of Ribs," *Applied Thermal Engineering*, vol. 31, no. 14-15, pp. 2702-2708, 2011. [CrossRef] [Google Scholar] [Publisher Link]

[11] B. Varun Kumar et al., "Enhancement of Heat Transfer in SAH with Polygonal and Trapezoidal Shape of the Rib Using CFD," *Energy*, vol. 234, 2021. [CrossRef] [Google Scholar] [Publisher Link]

[12] Karmveer et al., "An Experimental Study of Thermohydraulic Performance of Solar Air Heater Having Multiple Open Trapezoidal Rib Roughnesses," *Experimental Heat Transfer*, vol. 37, no. 3, pp. 313-333, 2024. [CrossRef] [Google Scholar] [Publisher Link]

[13] Anil Singh Yadav, and J.L. Bhagoria, "A CFD Based Thermo-Hydraulic Performance Analysis of an Artificially Roughened Solar Air Heater Having Equilateral Triangular Sectioned Rib Roughness on the Absorber Plate," *International Journal of Heat and Mass Transfer*, vol. 70, pp. 1016-1039, 2014. [CrossRef] [Google Scholar] [Publisher Link]

[14] Yadaba Mahanand, and Jnana Ranjan Senapati, "Thermal Enhancement Study of a Transverse Inverted-T Shaped Ribbed Solar Air Heater," *International Communications in Heat and Mass Transfer*, vol. 119, 2020. [CrossRef] [Google Scholar] [Publisher Link]

[15] Yash M. Patel, Sanjay V. Jain, and Vikas J. Lakhera, "Thermo-Hydraulic Performance Analysis of a Solar Air Heater Roughened with Discrete Reverse NACA Profile Ribs," *International Journal of Thermal Sciences*, vol. 167, 2021. [CrossRef] [Google Scholar] [Publisher Link]

[16] Yadaba Mahanand, and Jnana Ranjan Senapati, "Thermo-Fluid Analysis of a Pentagonal Ribbed Triangular Solar Air Heater Duct (TSAHD): A Three-Dimensional Numerical Investigation," *International Communications in Heat and Mass Transfer*, vol. 137, 2022. [CrossRef] [Google Scholar] [Publisher Link]

[17] Nitesh Dutt et al., "Thermo-Hydraulic Performance of Solar Air Heater having Discrete D-shaped Ribs as Artificial Roughness," *Environmental Science and Pollution Research*, pp. 1-22, 2023. [CrossRef] [Google Scholar] [Publisher Link]

[18] Kottayat Nidhul et al., "Enhanced Thermo-Hydraulic Performance in a V-Ribbed Triangular Duct Solar Air Heater: CFD and Exergy Analysis," *Energy*, vol. 200, 2020. [CrossRef] [Google Scholar] [Publisher Link]

[19] V.S. Hans, R.P. Saini, and J.S. Saini, "Heat Transfer and Friction Factor Correlations for a Solar Air Heater Duct Roughened Artificially with Multiple V-Ribs," *Solar Energy*, vol. 84, no. 6, pp. 898-911, 2010. [CrossRef] [Google Scholar] [Publisher Link]

[20] Dongxu Jin et al., "Numerical Investigation of Heat Transfer Enhancement in a Solar Air Heater Roughened by Multiple V-Shaped Ribs," *Renewable Energy*, vol. 134, pp. 78-88, 2019. [CrossRef] [Google Scholar] [Publisher Link]

[21] Adisu Bekele, Manish Mishra, and Sushanta Dutta, "Performance Characteristics of Solar Air Heater with Surface Mounted Obstacles," *Energy Conversion and Management*, vol. 85, pp. 603-611, 2014. [CrossRef] [Google Scholar] [Publisher Link]

[22] Madhukeshwara Nanjundappa, "Optimum Thermo-Hydraulic Performance of Solar Air Heater Provided with Cubical Roughness on the Absorber Surface," *Experimental Heat Transfer*, vol. 33, no. 4, pp. 374-387, 2020. [CrossRef] [Google Scholar] [Publisher Link]

[23] A. Leander Antony et al., "Influence of Stepped Cylindrical Turbulence Generators on the Thermal Enhancement Factor of a Flat Plate Solar Air Heater," *Solar Energy*, vol. 198, pp. 295-310, 2020. [CrossRef] [Google Scholar] [Publisher Link]

[24] H.S. Arunkumar, Shiva Kumar, and K. Vasudeva Karanth, "Analysis of a Solar Air Heater for Augmented Thermohydraulic Performance Using Helicoidal Spring Shaped Fins-A Numerical Study," *Renewable Energy*, vol. 160, pp. 297-311, 2020. [CrossRef] [Google Scholar] [Publisher Link]

[25] Parag Jyoti Bezbaruah, Rajat Subhra Das, and Bikash Kumar Sarkar, "Experimental and Numerical Analysis of Solar Air Heater Accoutered with Modified Conical Vortex Generators in a Staggered Fashion," *Renewable Energy*, vol. 180, pp. 109-131, 2021. [CrossRef] [Google Scholar] [Publisher Link]

[26] A. Saravanan et al., "Thermo-Hydraulic Performance of a Solar Air Heater with Staggered C-Shape Finned Absorber Plate," *International Journal of Thermal Sciences*, vol. 168, 2021. [CrossRef] [Google Scholar] [Publisher Link]

[27] Sohan Lal Sharma et al., "CFD Analysis of Artificially Roughened Solar Air Heater: A Comparative Study of C-Shape, Reverse C-Shape, and Reverse R-Shape Roughness Element," *International Journal of Ambient Energy*, vol. 45, no. 1, 2024. [CrossRef] [Google Scholar] [Publisher Link]

[28] Leila N. Azadani, and Nadiya Gharouni, "Multi Objective Optimization of Cylindrical Shape Roughness Parameters in a Solar Air Heater," *Renewable Energy*, vol. 179, pp. 1156-1168, 2021. [CrossRef] [Google Scholar] [Publisher Link]

[29] Hassan A.H. Alzahrani et al., "Enhancing Solar Air Heater Efficiency with 3D Cylinder Shaped Roughness Elements," *Case Studies in Thermal Engineering*, vol. 51, pp. 1-17, 2023. [CrossRef] [Google Scholar] [Publisher Link]

[30] Abdulmohsen O. Alsaiari et al., "Heat Transfer Augmentation in a Solar Air Heater with Conical Roughness Elements on the Absorber," *Case Studies in Thermal Engineering*, vol. 36, pp. 1-14, 2022. [CrossRef] [Google Scholar] [Publisher Link]

[31] Vikash Kumar, and Ramesh Murmu, "Performance Based Investigation of Inclined Spherical Ball Roughened Solar Air Heater," *Applied Thermal Engineering*, vol. 224, 2023. [CrossRef] [Google Scholar] [Publisher Link]

Appendix 1. Uncertainty Analysis

Experimental tests invariably entail a degree of uncertainty, regardless of the meticulousness of their execution. Consequently, it is essential to ascertain the extent to which scientific measurements may be erroneous. The error analysis was conducted to estimate the uncertainty range of the experimental data.

This was accomplished by examining the dispersion of the utilized raw data. Kline and McClintock devised a method to ascertain the ambiguity of experimental data, which is employed in this study. The error in the measurement of "y" is determined when the value of any parameter is computed using specific measured values.

$$\frac{\delta y}{y} = \left[\left(\frac{\delta y}{\delta x_1}\delta x_1\right)^2 + \left(\frac{\delta y}{\delta x_2}\delta x_2\right)^2 + \cdots \left(\frac{\delta y}{\delta x_n}\delta x_n\right)^2\right]^{0.5}$$

Area of the Absorber Plate (Ap)

$$A_P = W \times L$$

$$\frac{\delta A_P}{A_P} = \left[\left(\frac{\delta A_P}{\delta L}\delta L\right)^2 + \left(\frac{\delta A_P}{\delta W}\delta W\right)^2\right]^{0.5}$$

$$\frac{\delta A_P}{A_P} = \left[\left(\frac{\delta L}{L}\right)^2 + \left(\frac{\delta W}{W}\right)^2\right]^{0.5}$$

$$\frac{\delta A_P}{A_P} = \left[\left(\frac{0.001}{1}\right)^2 + \left(\frac{0.00003}{0.31725}\right)^2\right]^{0.5}$$

$$\frac{\delta A_P}{A_P} = 0.001004 \; or \; 0.1004\%$$

Area of Flow (Ac)

$$\frac{\delta A_c}{A_c} = \left[\left(\frac{\delta A_P}{\delta W}\delta W\right)^2 + \left(\frac{\delta A_P}{\delta H}\delta H\right)^2\right]^{0.5}$$

$$\frac{\delta A_c}{A_c} = \left[\left(\frac{\delta W}{W}\right)^2 + \left(\frac{\delta H}{H}\right)^2\right]^{0.5}$$

$$\frac{\delta A_c}{A_c} = \left[\left(\frac{0.00003}{0.31725}\right)^2 + \left(\frac{0.00006}{0.03000}\right)^2\right]^{0.5}$$

$$\boldsymbol{\frac{\delta A_c}{A_c} = 0.00200223 \; or \; 0.2002\%}$$

Hydraulic Diameter (Dh)

$$\frac{\delta D}{D} = \left[\left(\frac{\delta D}{\delta W}\delta W\right)^2 + \left(\frac{\delta D}{\delta H}\delta H\right)^2\right]^{0.5}$$

$$\frac{\delta D}{D} = [(0.0149 \times 3 \times 10^{-5})^2 + (1.669 \times 3 \times 10^{-5})^2]^{0.5}$$

$$\frac{\delta D}{D} = 0.001827 \; or \; 0.1827\%.$$

Useful Heat Gain (Qu)

$$Q_u = m \times C_P \times (T_0 - T_i)$$

$$\frac{\delta Q_u}{Q_u} = \left[\left(\frac{\delta \dot{m}}{\dot{m}}\right)^2 + \left(\frac{\delta C_P}{C_P}\right)^2 + \left(\frac{\delta \Delta T}{\Delta T}\right)^2\right]^{0.5}$$

$$\frac{\delta Q_u}{Q_u} = [(0.01\,)^2 + (0.001)^2 + (0.0488)^2]^{0.5}$$

$$\frac{\delta Q_u}{Q_u} = 0.0498 \; or \; 4.98\%$$

Reynolds Number (Re)

$$\frac{\delta Re}{Re} = \left[\left(\frac{\delta \dot{m}}{\dot{m}}\right)^2 + \left(\frac{\delta \mu}{\mu}\right)^2 + \left(\frac{\delta D_h}{D_h}\right)^2\right]^{0.5}$$

$$\frac{\delta Re}{Re} = [(0.01)^2 + (0.01)^2 + (0.001827)^2]^{0.5}$$

$$\frac{\delta Re}{Re} = 0.0142 \; or \; 1.43\%$$

Prandtl Number (Pr)

$$\frac{\delta Pr}{Pr} = \left[\left(\frac{\delta k}{k}\right)^2 + \left(\frac{\delta \mu}{\mu}\right)^2 + \left(\frac{\delta C_P}{C_P}\right)^2\right]^{0.5}$$

$$\frac{\delta Pr}{Pr} = [(0.0003694)^2 + (0.01)^2 + (0.001)^2]^{0.5}$$

$$\frac{\delta Pr}{Pr} = 0.010056 \; or \; 1.0056\%$$

Nusselt Number (Nu)

$$\frac{\delta Nu}{Nu} = \left[\left(\frac{\delta k}{k}\right)^2 + \left(\frac{\delta h}{h}\right)^2 + \left(\frac{\delta D_h}{D_h}\right)^2\right]^{0.5}$$

$$\frac{\delta Nu}{Nu} = [(0.0003694)^2 + (0.05573)^2 + (0.001827)^2]^{0.5}$$

$$\frac{\delta Nu}{Nu} = 0.05579 \; or \; 5.579\%$$

Friction Factor (f)

$$\frac{\delta f}{f} = \left[\left(\frac{\delta \Delta P}{\Delta P}\right)^2 + \left(\frac{\delta L}{L}\right)^2 + \left(\frac{\delta D_h}{D_h}\right)^2 + \left(2\frac{\delta V}{V}\right)^2\right]^{0.5}$$

$$\frac{\delta f}{f} = [(0.00423)^2 + (0)^2 + (0.001827)^2 + 2 \times (0.01075)^2]^{0.5}$$

$$\frac{\delta f}{f} = 0.02198 \; or \; 2.20\%$$

Table 6. Uncertainty values of operating parameters

Sr. No	Parameters	Uncertainty
1	Area of the absorber plate (Ap).	0.1004%
2	Area of flow (Ac).	0.2002%
3	Hydraulic diameter (Dh)	0.1827%.
4	Useful heat gain (Qu)	4.98%
5	Reynolds Number (Re)	1.43%
6	Prandtl number (Pr)	1.0056%
7	Nusselt number (Nu)	5.579%
8	Friction factor (f)	2.20%

Appendix 2. Graphical Abstract

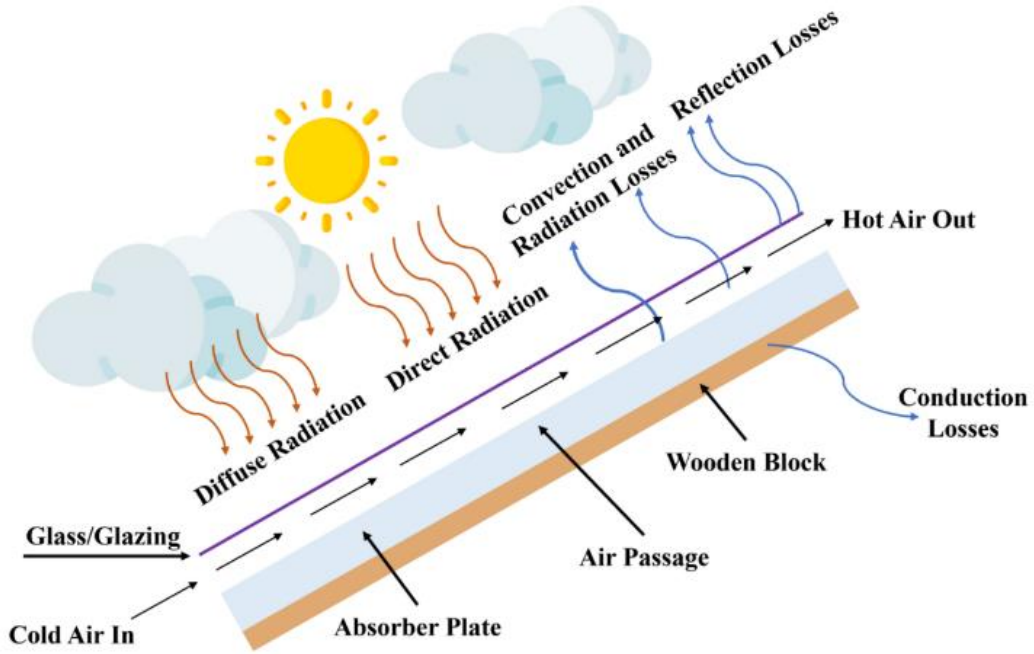

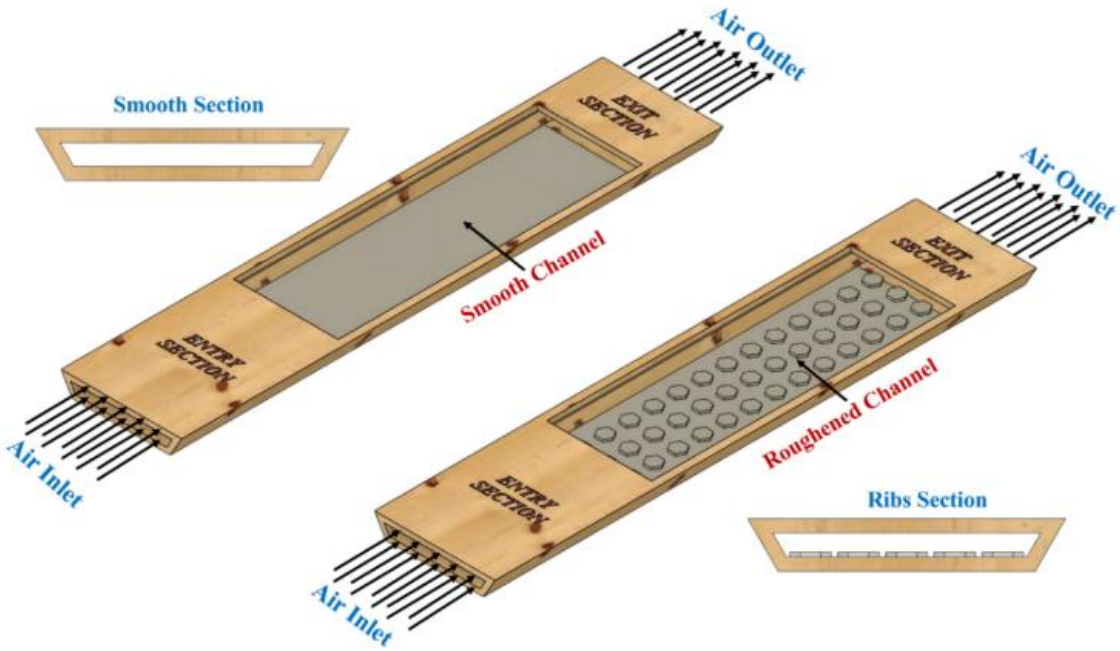

Abbreviations and Acronyms

T_i = Temp. of Air at entry (°C)
T_o = Temp. of Air at exit (°C)
W Width of Duct
H= Height of Duct
ρ = density of Air
V = Air velocity.
μ = Viscosity of Air

m = Air mass flow rate (kg/s)
C_p = Specific heat of Air at static pressure (kJ/kg-K)
Q = Heat gained/received by Air, Watt.
A_p = Area of the absorber sheet, m^2
T_{pm} = Average Temp. of sheet, °C.
T_{fm} = Average Temp. of fluid flowing, °C
h = Convective heat transfer coefficient (W/m^2-K)
D_h = Hydraulic dia. of quadratic duct, m
k = Thermal Conductivity of the flowing fluid (W/m-K)
ΔP = Pressure drop
L Length of duct
V= Velocity of Air
Nu & Nu_s =Nusselt no. of rough and smooth plate
f & f_s =friction factor of rough and smooth plate
BR= Blockage ratio
Re= Reynolds Number